Catalysis Letters (2023) 153:1916–1931
https://doi.org/10.1007/s10562-022-04106-z

# Theoretical Study on the Efficient Electrocatalytic $N_2$ Reduction Reaction of Bimetallic Single Atom Embedded in Phthalocyanine

**Lingxiao Jiao**[1] · **Ling Guo**[1]

Received: 26 April 2022 / Accepted: 2 July 2022 / Published online: 5 September 2022
© The Author(s), under exclusive licence to Springer Science+Business Media, LLC, part of Springer Nature 2022

## Abstract

Electrocatalytic nitrogen reduction is a new method of ammonia synthesis instead of Haber–Bosch process, which consumes less energy and is environmentally friendly. The N≡N bond can be weakened by the coordination of bimetal atoms in the presence of bimetallic sites, thus enhancing NRR activity. In this paper, we systematically studied different diatomic catalysts by density functional theory, and screened out some suitable candidate catalysts, Finally, it is concluded that FeTi@Pc catalyst has the best catalytic activity with the limiting potential of − 0.37 V and selectivity for NRR reaction. We firmly believe that this work not only open up a way for the design of other non-noble metal NRR electrocatalysts with high activity, but also provide a promising strategy for the synthesis of NRR catalysts in experiments.

### Graphical Abstract

We used 3d and 4d transition metal atoms to replace N atoms and Fe doped on the Phthalocyanine as the electrocatalyst for NRR. After screening and research, we found that FeTi@Pc catalyst has good catalytic activity and selectivity for NRR.

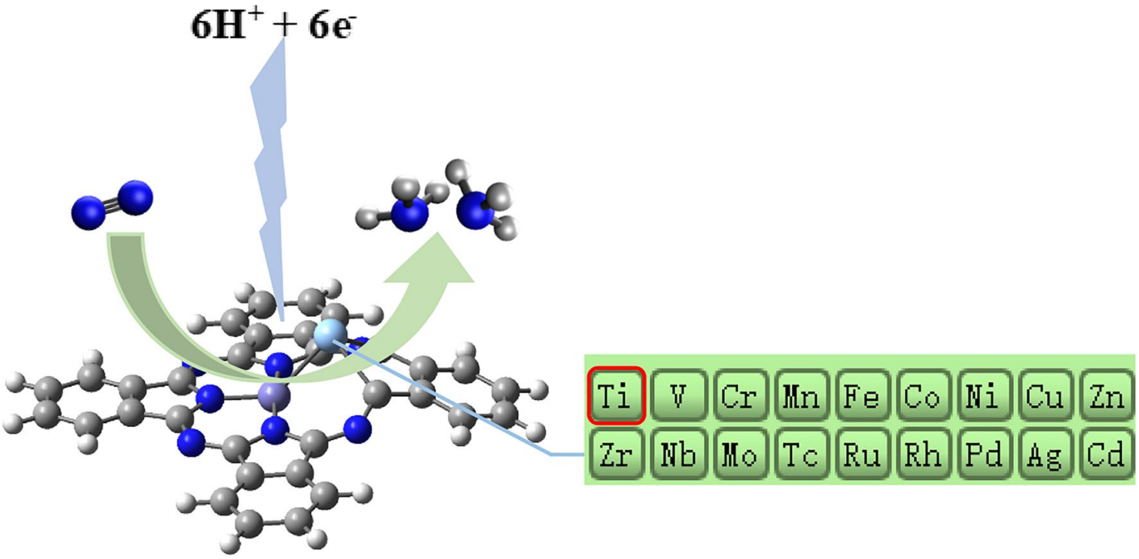

**Keywords** Double transition metal atoms · $N_2$ reduction reaction · DFT · Synergy effect

---

✉ Ling Guo
1413435212@qq.com

[1] Key Laboratory of Magnetic Molecules & Magnetic Information Materials, Ministry of Education, The School of Chemistry and Material Science, Shanxi Normal University, Taiyuan 030000, China

## 1 Introduction

Ammonia, as an indispensable chemical in human production activities, plays an irreplaceable role in the production of plastics, fibers, fertilizers, fuels, medicines and other processes [1]. In addition, because its combustion products are nitrogen and water, which already exist in nature, ammonia can also be used as a clean energy carrier [2, 3]. Due to the important role of ammonia, its consumption is also large. With the development of various fields, the demand for ammonia will also increase. At present, the main industrial ammonia production is the Haber–Bosch technology, which combines nitrogen and hydrogen under high temperature and pressure in the presence of an iron-based catalyst [4, 5]. In this process, high temperatures and pressures consume about 2% of the world's energy each year [6], The pure hydrogen used in the reaction, which does not exist in nature, is mainly obtained through steam reforming of fossil fuels (such as natural gas). This process not only consumes about 5% of the world's total energy from natural gas, but also produces a large amount of $CO_2$, which is not beneficial to the improvement of ecological environment [7]. Therefore, in order to alleviate the high energy consumption and lower environmental pollution of industrial synthesis, it is necessary to develop a mild and environmentally friendly ammonia synthesis method.

In recent years, the electrocatalytic nitrogen reduction reaction technology for ammonia synthesis has been considered as a promising and potential method to replace Haber–Bosch technology [8]. Compared with traditional industrial technology, electrocatalytic NRR is carried out under normal temperature and pressure, with mild reaction conditions, higher production efficiency possible than the HB method, low energy consumption, and low cost. It uses nitrogen and water as raw materials to avoid the consumption of fossil fuels and reduce greenhouse gas emissions. Therefore, the electrocatalytic nitrogen reduction reaction of ammonia synthesis technology has been a research focus of the majority of scholars. However, under environmental conditions, the reduction of inert nitrogen to ammonia needs to solve several problems: 1. $N_2$ has extremely high stability and inertness,since the first bond breaks require high thermodynamic energy (410 kJ/mol) and bond energy (945 kJ/mol), it is difficult to dissociate the N≡N bond; 2. The negative electron affinity (− 1.8 eV) and low proton affinity (5.12 eV) and high ionization potential (15.85 eV) of $N_2$ can reduce the reactivity; 3. Its large HOMO–LUMO energy gap (10.82 eV) hinders electron transfer to a certain extent. 4. Before the N–N bond breaks, the first H atom adds to the high enthalpy of $N_2H^+$ ($\Delta H^0 = +37.6$ kJ/mol) [9–11]. Based on these issues, it is necessary to design a catalyst that can reduce the activation energy of the reaction and weaken the N≡N bond energy to promote the synthesis of $NH_3$. In the process of synthesizing $NH_3$, there are also several difficulties. For example: 1. $N_2$ adsorption and $NH_3$ desorption on the catalyst surface; 2. Selectivity between NRR reaction and HER reaction, etc. [12, 13]. Therefore, the development of electrocatalysts with high activity, high selectivity, and the ability to adjust NRR and HER competition at room temperature is the key to realization of e-NRR.

Up to now, with the rapid development of theoretical methods and experimental techniques, many electrocatalysts have been designed for NRR [14–27]. Among them, scholars have conducted extensive research on single-atom catalysts, diatomic catalysts and other transition metal atom catalysts [28–40]. For example, Geng [41] and Tao [42] independently reported that a single ruthenium site supported on nitrogen-doped porous carbon has high activity for the electro-reduction of aqueous solutions to $NH_3$ under ambient conditions. At the same time, Lu et al. [43] synthesized an atom-dispersed single molybdenum catalyst on g-$C_3N_4$ for electrochemical synthesis of $NH_3$ under environmental conditions. And the experimental results of Zang et al. [44] showed that a single copper atom embedded in porous carbon exhibits good catalytic performance. Although the active center of monatomic catalyst is favorable for the subsequent electron and protic process, it is difficult to release the second $NH_3$ and has a very high initial potential. Therefore, researchers learned from the experience of diatomic catalysts used for hydrogen evolution (HER), $CO_2$ reduction reaction ($CO_2$RR), oxygen evolution reaction (OER) and oxygen reduction reaction (ORR) [45–52], and designed a diatomic catalyst for NRR [53–55]. Among them, Zhao et al. [50] re-examined the catalysis of ORR by 10 cobalt-based diatomic catalysts CoMN$_6$-gra (M = Sc, Ti, V, Cr, Mn, Fe, Co, Ni, Cu, Zn) through first-principles calculations. performance, emphasizing that the magnetic coupling between transition metal atoms can have an impact on the binding strength, potential determining step, and limiting potential between intermediates and DACs, and demonstrating that manipulating the magnetic coupling between transition metal atoms is the key to improving the electrocatalytic activity of DACs an emerging and effective way. The above conclusions also apply to NRR. He et al. [53] proved that catalysts with bimetallic active sites could weaken N≡N bond and adjust the binding strength of key intermediates through strong polarization to improve the activity of NRR. Diatomic catalysts not only have the advantages of SACs, but also have higher metal atom loading and more flexible active sites [54].

Phthalocyanine ($H_2$Pc) is a kind of synthetic compound with 18 electron macroring conjugated system similar to porphyrins which are widely found in nature. Phthalocyanine has high stability to light, heat and even acid and alkali, and has strong coordination ability. It can react with almost all metal elements to form metal complexes with special colors, commonly known as metal phthalocyanines (MPc), due to its high catalytic activity and good selectivity, has been extensively studied and used in catalytic oxygen reduction reactions [56–59], as well as in applications such as catalysis and environmental protection, solar cells, medical and health care [60–63]. In the chemical industry, researchers have explored the catalytic application of it for various reactions, among which the main product is CO. For example, Zhang et al. [64] found that cobalt phthalocyanine molecules uniformly supported on carbon nanotubes can efficiently catalyze the reduction of $CO_2$ to CO, and in particular, the introduction of cyanide can further improve its catalytic performance. Han et al. [65] later found that the polymerized Fe-PC and carbon nanotube composite catalyst cleverly combined the advantages of homogeneous and heterogeneous catalysts, with a high efficiency of CO Faraday Efficiency. However, there are few studies on the use of metal phthalocyanine catalysts for electrocatalytic NRR reaction, so this paper uses it as the catalyst base for e-NRR.

Iron is a cheap and abundant metallic element on earth, and also an important element for fixing $N_2$ in nitrogenase. At the same time, in the HB process, Fe is widely used as the best pure metal catalyst [66]. Norskov et al. [67] calculated the catalytic activity trends of a series of transition metal surfaces and applied potentials. The results proved that Fe, Rh, and Ru are at the top of the volcano map, indicating that a large amount of ammonia can be expected to be produced on these metals. Considering the low cost and wide storage capacity of iron, iron has more obvious advantages than precious metals in practical applications. Compared with precious metals, iron not only has low cost, but also has the characteristics of abundant content, wide storage capacity and uses, so in practical applications, iron has obvious advantages. In addition, there are many experiments and theoretical studies that can prove the high catalytic activity of monoatomic iron catalysts [68–72]. In order to further improve the catalytic activity of the single-atom iron catalyst for NRR, we tried to construct a FeTMs@Pc catalyst to study the possibility of its catalytic $N_2$ reduction reaction.

In this work, we studied a series of Fe and 3d,4d transition metals co-doped on phthalocyanine substrates (written as FeTMs@Pc) by density functional theory calculations as electrocatalysts for NRR. First of all, after different theoretical calculations, the most stable FeTMs@Pc structure was constructed, and the established catalysts were initially screened. We concluded that there were five heteronuclear BACs (FeTi@Pc, FeV@Pc, FeCu@Pc, FeCr@Pc and FeTc@Pc) that could improve the catalytic activity of NRR. After subsequent research and comparative analysis of these five candidate catalysts, the optimal catalyst, FeTi@Pc, was found to attract attention with a low limit potential of − 0.37 V by the distal mechanism, and could avoid HER competitive reaction well, with better NRR selectivity.

## 2 Calculation Methods

For the structure of all the catalysts involved in this article, All the geometric optimizations were carried out by spin-polarized DFT method in the generalized gradient approximation (GGA) of Perdew-Burke-Ernzerhof (PBE), as implemented in Gaussian 09 backage [73]. The non-metal atoms (C, N, H atoms) in the structure use the 6–31 g* basis set, and the metal atoms use the Los Alamos National Laboratory 2 Double Zeta (LANL2DZ) basis set. The valence layer orbital of the transition metal atom LANL2DZ includes a total of three s-basis functions, three p-basis functions and two d-basis functions. When the LANL2DZ basis set treats (n-1) s and (n-1) p orbitals as price layer orbitals, the calculation accuracy can be significantly improved [74].

The Gibbs free energy change of each basic step of $N_2$ adsorption is calculated using the calculated hydrogen electrode model proposed by Nørskov et al. [75] CHE uses half of the chemical potential of $H_2$ as the chemical potential of the proton-electron ($H^+/e^-$) pair:$\mu_{H^+} + \mu_{e^-} = \frac{1}{2}\mu_{H_2}$. The free energy change ($\Delta G$) of each protonation hydrogenation step was computed according to:

$$\Delta G = \Delta E + \Delta E_{ZPE} - T\Delta S + \Delta G_U + \Delta G_{pH}$$

where $\Delta E$ is the reaction energy obtained by DFT computations, $\Delta E_{ZPE}$ is the change of zero-point energy, the calculation can be as follows: $E_{ZPE} = 1/2 \sum_{i=1}^{N_{modes}} hv_i$, Where $N_{modes}$ is the number of vibration modes. T is the temperature (298.15 K) and $\Delta S$ is the change in entropy. The entropies of the gas phase were taken from the NIST database. Based on the vibrational frequencies,the entropies and zero-point energy of the adsorbates were calculated, and the entropy can be determined as follows [76]:

$$S(T) = \sum_{i=1}^{3N}[-R\ln(1 - e^{-hv_i/k_BT} + \frac{N_A hv_i}{T}\frac{e^{-hv_i/k_BT}}{1 - e^{-hv_i/k_BT}}]$$

where $R$ is the molar gas constant, h is the Planck constant, $k_B$ is the Boltzmann constant, $N_A$ is the Avogadro number, $\nu_i$ is the normal mode frequency, and $N$ is the number of adsorbed atoms. $\Delta G_U$ could be calculated with $\Delta G_U = -eU$, where $e$ represents the transferred charge and U represents the potential on the electrode. $\Delta G_{pH}$ is the correction of $H^+$ free energy by concentration, which can be expressed as $\Delta G_{pH} = k_BT\ln 10 \times pH$. In this study the pH value was set to 0 to simulate a strong acidic environment (0.10 M HCl solution is the commonly used NRR electrolyte in experiments) [54]. According to Nørskov et al. [75] the thermodynamic activation barrier is equal to the maximum free energy difference. That is, the reaction potential determination step (PDS) is the basic chemical step with the maximum reaction free energy ($\Delta G$) and the minimum limiting potential ($U_L$).

Nørskov et al. used and investigated similar scheme for the stability of key adsorbents *OH (0.5 eV) and *OOH (0.25 eV) in the ORR mechanism. It was found that the stabilities of *NH, *NH and $*NH_2$ were 0.1, 0.1 and 0.2 eV, respectively (the limiting potential affecting the reaction intermediates was 0.1 eV). Moreover, the similarity in the corrections indicates that the shifts in activity should correspond to the shifts along the scaling; therefore, the fundamental limitations are not change significantly just by interacting with $H_2O$ [77, 78]. Based on the above, the influence of solvation was not considered.

## 3 Results and Discussion

### 3.1 Catalyst Screening Process

The $N_2$ reduction reaction is a relatively complicated process ($N_2 + 6H^+ + 6e^- = 2NH_3$), and its initial potential is determined by six electrochemical steps [67, 79]. $N_2$ can be adsorbed on the surface of the catalyst through two different configurations (end-on or side-on configuration), so the mechanism of NRR is uncertain. In general, in order to fully illustrate the NRR activity of the selected catalyst, 16 kinds of reaction intermediates should be considered [80]. In this context, a large-scale screening of NRR catalysts with high activity with computational high-throughput methods will consume or even waste huge computational resources. Therefore, it is necessary to use simple descriptors or adopt effective filtering strategies. Many research results in the past have concluded that a catalyst with a very low limiting potential can stably adsorb $N_2H$ and unstable $NH_2$. In other words, regardless of the mechanism, they have two parts —— the first hydrogenation step ($*N_2 + H^+ + e^- = *N_2H$) and the last hydrogenation step ($*NH_2 + H^+ + e^- = *NH_3$), these two hydrogenation steps are the most likely rate-determining steps in the whole process. Therefore, we use these two reaction steps as the criteria for rapid screening of the best NRR catalysts ($\Delta G_{N2\text{-}N2H}$ and $\Delta G_{NH2\text{-}NH3}$) [54, 80, 81]. We first calculated the free energy changes of the first and last hydrogenation steps for the seventeen types of FeTMs@Pc as a preliminary evaluation of the entire NRR process. Figure 1 displays the Gibbs free energy changes for the first and last hydrogenation steps on the 17 kinds of catalysts. In this figure, the horizontal and vertical axes represent the values of $\Delta G_{NH2\text{-}NH3}$ and $\Delta G_{N2\text{-}N2H}$, respectively. For the first hydrogenation step, we calculated the two different adsorption configurations including end-on and side-on configurations (as shown in Table S1). After comparison, we chose the smaller $\Delta G_{N2\text{-}N2H}$ value. Therefore, only those species near the lower left corner will have the better NRR catalytic activity. As can be seen from Fig. 1, there are five catalysts showing excellent catalytic activity (values of $\Delta G_{NH2\text{-}NH3}$ and $\Delta G_{N2\text{-}N2H}$ are lower than 0.65 eV) [53]. Therefore, we selected these five catalysts (marked in red triangle) to further evaluate their entire NRR catalytic activity, namely Fe–Ti, Fe–V, Fe–Cu, Fe–Zr and Fe–Tc.

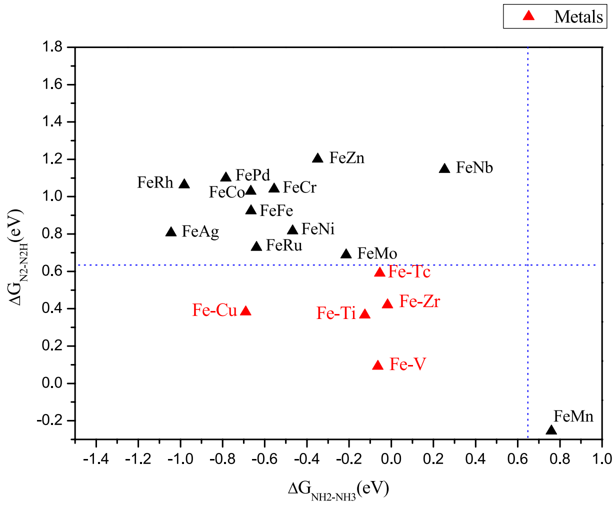

**Fig. 1** The Gibbs free energy changes of the first and last hydrogenation steps of NRR on different FeTMs@Pc DACs were calculated. The blue dashed line represents the value of 0.65 eV. The ones marked in red are the most promising NRR catalysts

### 3.2 Catalyst Structure Model

Jiang et al. researched the catalytic activity of a series of N-coordinated DMSCs by DFT calculations using the charge transfer, the average charge on the metal, the average d orbital center on metals, and the stretching vibration frequency of reactants as electron/spectral descriptors. They found that among the various metal combinations, the model of the $N_3$-adjacent bimetallic and iron-containing combination had stronger synergistic and kinetic effects, resulting in a much higher catalytic activity than other studies. Inspired by the experimental study, we designed the catalyst structure model (FeTMs@Pc) as shown in Fig. 2 [82]. The distance between Fe and another transition metal atom can be shortened by replacing the N atom of the nearest Fe atom with the transition metal atom in the Pc base, and the synergistic effect of the bimetal atom can be better played. We prove through calculation that the structure shown in Fig. 2 has the lowest energy and is the most stable structure. The structure of different FeTMs@Pc catalysts has different degrees of deformation, which is mainly due to the difference in the radius of the metal atoms, indicating that doping with different transition metal atoms can significantly control the geometric structure of FeTMs@Pc (The structures of all catalysts and their energies of high and low spin are shown in Table S2). Thus, doping with different transition metal

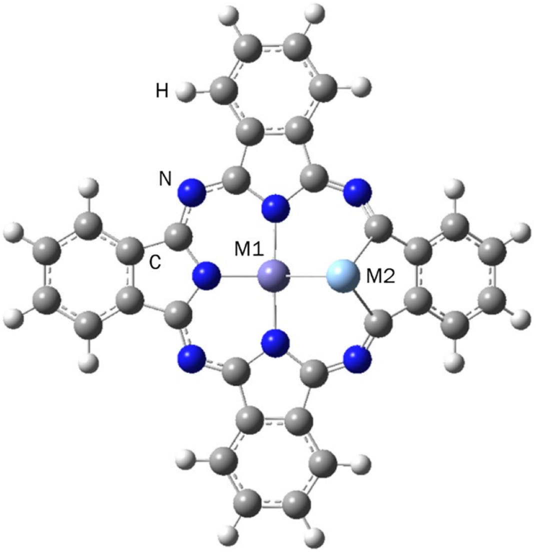

**Fig. 2** Top view of FeTMs@Pc DACs structure model

atoms provides a way to further promote NRR activity [53, 54].

Next, we investigated the stability and experimental feasibility of these catalyst systems by their binding energies ($E_b$) and formation energies ($E_f$). The formula for calculating the binding energy is: $E_b = E_{Pc+Fe} - \mu_N + E_{TM} - E_{FeTMs@Pc}$. $E_{Pc+Fe}$ is the energy of the Pc substrate doped with Fe atom, $E_{TM}$ is the energy of the isolated transition metal atom, and $E_{FeTMs@Pc}$ is the energy of the FeTMs@Pc catalyst system. If the obtained binding energy is negative, it indicates that the formed catalyst system has good thermodynamic stability. As can be seen from the Fig. 3a, the binding energies of the catalysts are all much less than 0 eV, indicating that the FeTMs@Pc catalysts have good stability. $E_f$ can well describe the formation possibilities of a particular catalyst system, mainly because the value of $E_f$ is related to the energy (chemical potential) of each species, which depends on the experimental conditions [33]. In order to characterize the experimental possibility of our designed catalyst, the formation energy of the catalyst was calculated according to the following formula: $E_f = E_{FeTMs@Pc} + \mu_N - (E_{Pc} + E_{Fe} + E_{TM})$. $E_{Pc}$ is the energy of a single phthalocyanine molecule, and $E_{Fe}$ is the energy of Fe atom. As shown in Fig. 3b, except that the formation energies of FeZn@Pc and FeAg@Pc are positive, which are 1.03 eV and 0.41 eV, respectively. The formation energies of other catalysts range from about − 0.87 to − 6.50 eV, indicating the thermodynamic stability of these catalyst systems, and it can also be said that these catalyst systems have the possibility of experimental synthesis. In addition, we also evaluated the electrochemical stability of FeTMs@Pc by calculating the dissolution potential ($U_{diss}$), which is defined as $U_{diss} = U^0_{diss}(\text{metal, bulk}) - E_f/ne$. $U^0_{diss}$(metal, bulk) and $n$ are the standard dissolution potential of the bulk metal and the coefficient for the aqueous dissolution reaction, respectively. According to some references definitions [77, 83, 84], materials with $U_{diss} > 0$ V are considered electrochemically stable. Table S3 lists the exact values of $U_{diss}$. Among them, the dissolution potentials of FeZn@Pc, FePd@Pc, and FeAg@Pc catalysts are less than 0 V. The other catalysts are all greater than 0 V. The above results show that most of our catalyst systems are thermodynamically and electrochemically stable, which demonstrates the reliability and feasibility of FeTMs@Pc catalysts.

In order to further study the binding mechanism of Fe-TM on the Pc substrate, the projected density of states (PDOS) of the five selected FeTMs@Pc (FeTi@Pc, FeV@Pc, FeCu@Pc, FeZr@Pc and FeTc@Pc) were calculated, as shown in Fig. 4. The 3d orbital of iron atom, the 3d or 4d of TM, the 2p of C atom and the 2p of N atom are marked with black, pink, blue and green lines, respectively,

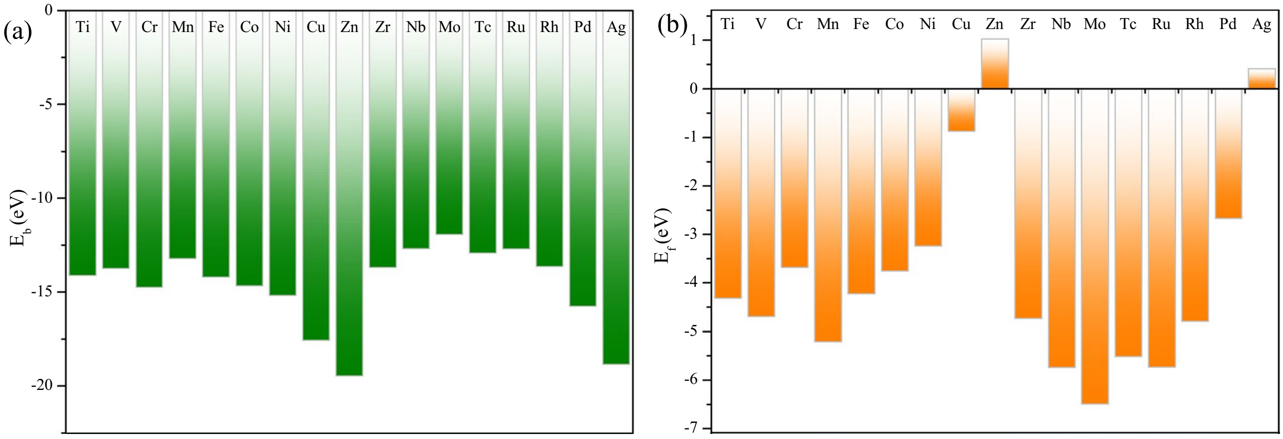

**Fig. 3** **a** The binding energy ($E_b$) of the FeTMs@Pc catalyst systems; **b** The formation energy ($E_f$) of the FeTMs@Pc catalyst systems

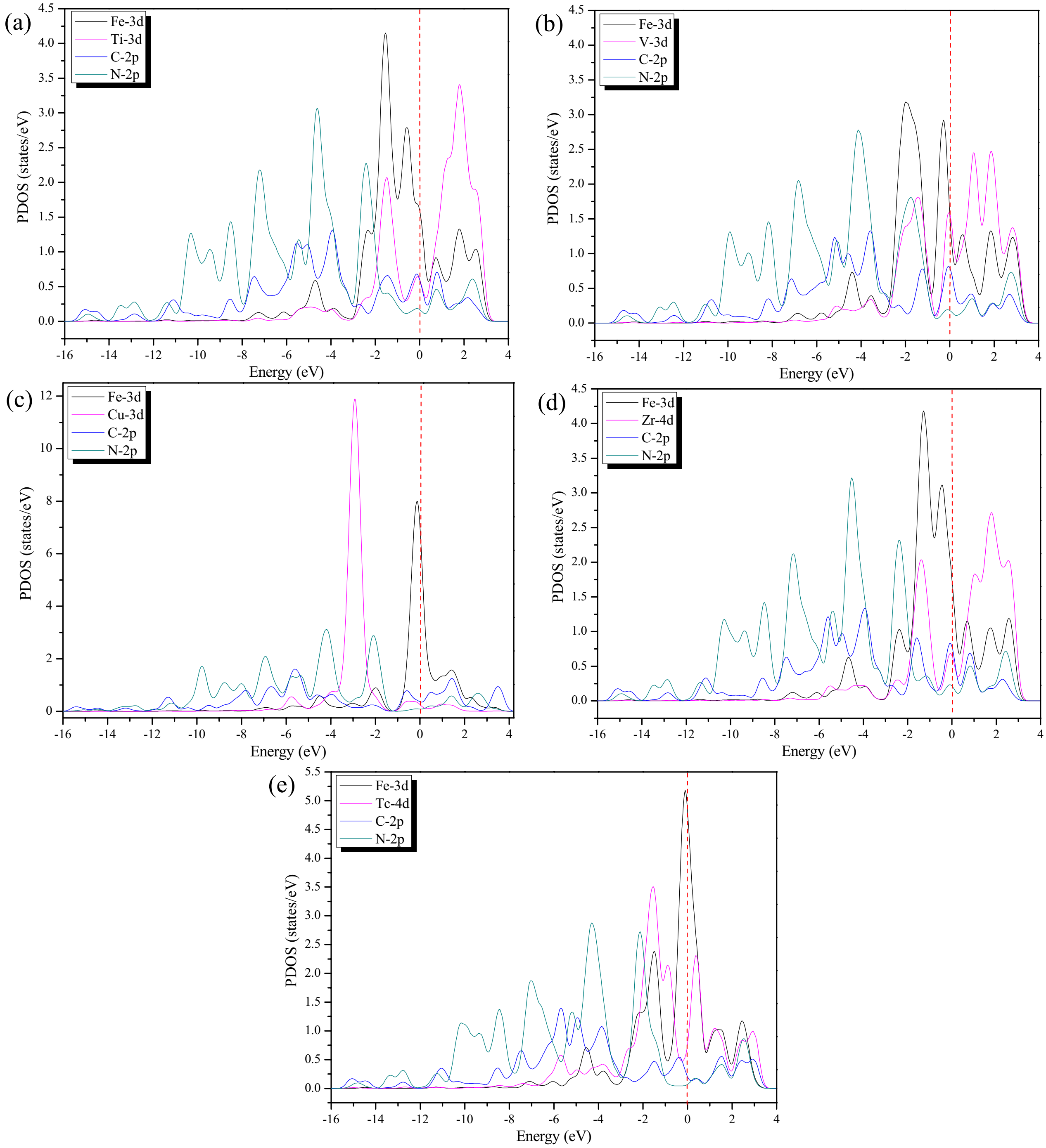

**Fig. 4** The projected density of states (PDOS) of catalyst

and the red dotted line represents the Fermi energy level with a value of 0 eV. Except for FeCu@Pc, the obvious orbital hybridization between Fe(3d), TM(3d/4d), C(2p) and N(2p) indicates that Fe-TM dimer can be firmly fixed to the substrate by strong covalent bonds with C/N atoms, and also indicates that the catalyst system has excellent stability. More interestingly, except for FeCu@Pc, the d-band centers of two metal atoms in the other four catalysts are closer to the Fermi level. (See Fig. S1). According to the d-band center theory [85, 86], the interaction between the adsorbate energy level and the d-band (narrow band) can form bonding orbitals/anti-bonding orbitals.If the energy level of the d-band center is closer to the Fermi level, the ability of its surface to adsorb reaction intermediates is enhanced, which can improve the activity of NRR. So we think that FeTi@Pc may have higher $N_2$ activation activity.

### 3.3 Adsorption of $N_2$ on FeTMs@Pc

The adsorption and activation of $N_2$ on the catalyst is the first step of the entire catalytic reaction, because the reduction of $N_2$ to $NH_3$ is a rather complicated process, which involves a variety of reaction mechanisms, so the adsorption of $N_2$ on the surface of the electrocatalyst activates the inert $N_2$ and the subsequent reduction process [87]. Therefore, we studied the adsorption configuration of $N_2$ molecule on 17 kinds of FeTMs@Pc catalysts. According to the adsorption configuration of $N_2$ molecule, it can be divided into two categories: end-on configuration and side-on configuration, as shown in Fig. 5. Here, end-on means that one end of the $N_2$ molecule is attached to the active site of the catalyst, and side-on refers to the adsorption of two ends of the $N_2$ molecule on the active site of the catalyst. $N_2$ can be adsorbed in end-on adsorption mode on all catalysts, interestingly, it can also be adsorbed on FeV@Pc, FeMn@Pc and FeRu@Pc catalysts in side-on configuration, and on other catalysts, the side-on configuration will be transformed into end-on configuration after optimization (All of the adsorption configurations are shown in Table S1). In addition, in order to confirm that $N_2$ can really adsorb on metal sites, we also calculated $N_2$ adsorption on other possible sites, such as C and N atoms near near two metal atoms. The results showed that after optimization, nitrogen were adsorbed on the metal double sites, rather than any other sites. This provided a structural basis for subsequent reduction of nitrogen on the metal double sites.

It is important to study the bonding mechanism of $N_2$ on FeTMs@Pc catalyst surface. $N_2$ can be adsorbed on the catalyst surface mainly due to orbital hybridization and electron transfer. In order to study the interaction of $N_2$ on the surface of FeTMs@Pc metal dimer and $N_2$ from the aspect of orbital hybridization, the projected density of states (PDOS) of the adsorption system was plotted, as shown in Fig. 6 (Take the five kinds of selected catalysts as examples). In Fig. 6, the densities of states for Fe's d orbital, TM's d orbital and N's p orbital are drawn with pink, black and blue lines, respectively. The red dotted line represents the Fermi level, which has a value of 0 eV. Near the Fermi level, there is a significant hybrid peak between the metal dimer (d) and nitrogen (p), indicating that orbital hybridization contributes to the bonding process of surface $N_2$ to some extent. In detail, the ability of FeTMs@Pc to adsorb/activate $N_2$ is mainly due to its unoccupied and occupied d orbitals. On the one hand, the unoccupied d orbitals of FeTMs@Pc accept electrons from the 2π and 3σ molecular orbitals of $N_2$ to form a bonded state to desorb and activate $N_2$. On the other hand, the occupied d orbitals feedback electrons to the 2π* orbitals of $N_2$ molecule, resulting in the formation of the partially occupied 2π* orbitals.

In order to study whether the electron transfer occurs the adsorption of $N_2$ on the surface, the electron density difference between the two configurations of $N_2$ adsorption on FeTMs@Pc is plotted, as shown in Fig. 7a (Take FeTi@Pc as an example). In Fig. 7a, charge accumulation and charge transfer are represented in blue and yellow regions, respectively. As can be seen from the charge density difference diagram, electron density transfer mainly occurs in the region of Fe atom and N–N bond, the accumulation of electron density mainly occurred in the region of Fe–N bond. This indicates that iron atoms act as electron donors during $N_2$ adsorption process, the strength of N≡N bond is weakened and the Fe–N bond is strengthened with electron transfer. In other words, as shown in Fig. 7b, FeTMs@Pc can "push" electrons into the anti-bonding orbital of $N_2$ while "pulling" the lone pair of electrons from $N_2$ at the same time. The synergistic effect of these two processes can significantly weaken the strong N≡N bond, laying the foundation for the subsequent multi-step reduction to generate ammonia molecules. All in all, $N_2$ is activated by electron transfer, leading to a significant extension of the N≡N bond in each $N_2$ adsorption configuration. (N–N bond lengths before and after $N_2$ adsorption are shown in Table S4).

### 3.4 Reaction Mechanism and Analysis

In order to further confirm the excellent performance of FeTMs@Pc as an electrocatalyst for converting $N_2$ into available $NH_3$, the entire NRR process (six proton-electron pair transfer reactions) of the five kinds of selected catalysts was studied. Among the five kinds of selected catalysts, except for FeV@Pc catalyst, which has two configurations for $N_2$ adsorption, the other four kinds of catalysts can only adsorption $N_2$ with end-on configuration. In previous

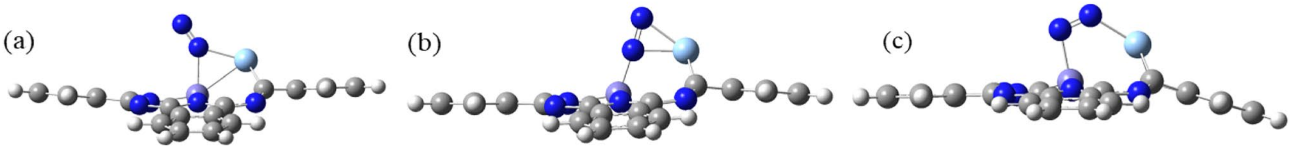

**Fig. 5** **a** end-on configuration of $N_2$ adsorption on FeTMs@Pc catalysts (TM = Ti-Zn, Zr-Ag); **b** side-on configuration of $N_2$ adsorption on FeTMs@Pc catalysts (TM = V, Mn); **c** side-on configuration of $N_2$ adsorption on FeTMs@Pc catalysts (TM = Ru)

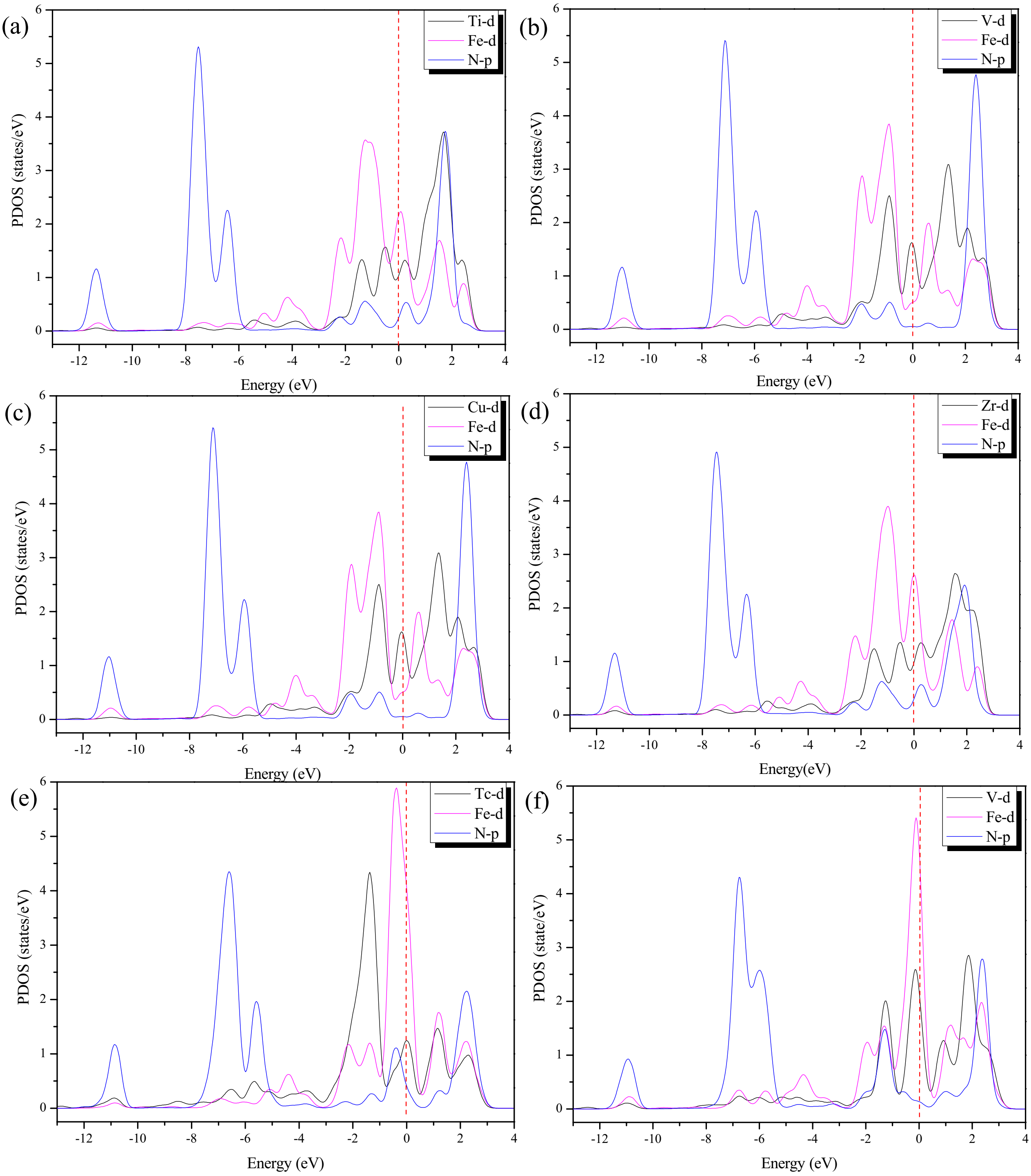

**Fig. 6** The Projected Density of states (PDOS) of **a** FeTi@Pc, **b** FeV@Pc, **c** FeCu@Pc, **d** FeZr@Pc, and **e** FeTc@Pc catalyst with end-on configuration and **f** FeV@Pc catalyst with side-on configuration for $N_2$ adsorption

studies [21, 88], the mechanism of nitrogen reduction reaction (NRR) on heterogeneous catalysts has been well established, and it is thought to be carried out through four main catalytic mechanisms, namely distal, alternating, continuous and enzymatic, as shown in Fig. 8. Among them, the end-on adsorption configuration promotes the subsequent reduction reaction through the distal and alternate pathways, while the enzymatic and continuous pathways start from the side-on adsorption configuration. Through the distal and continuous mechanism, the proton-electron pair first continuously

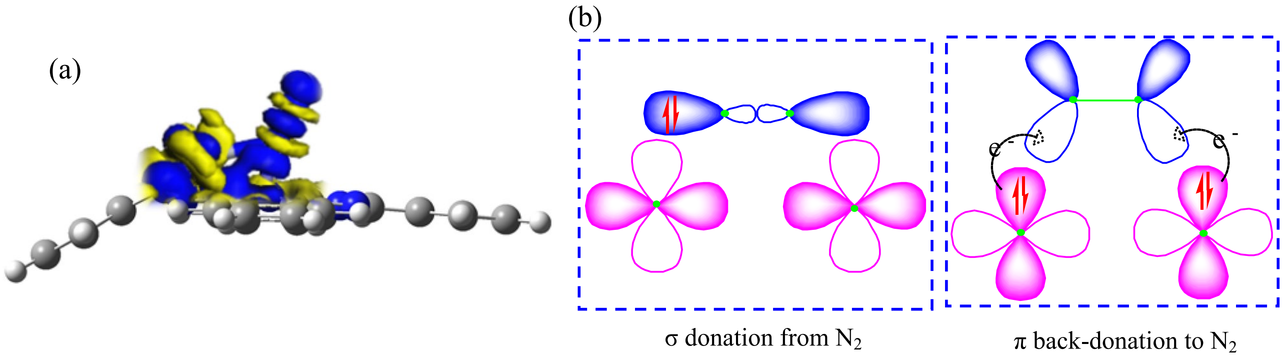

**Fig. 7** **a** The charge density difference of FeTi@Pc (Blue and yellow indicate charge accumulation and charge transfer, respectively); **b** Simplified schematic diagram of $N_2$ bonding to dual-site transition metals

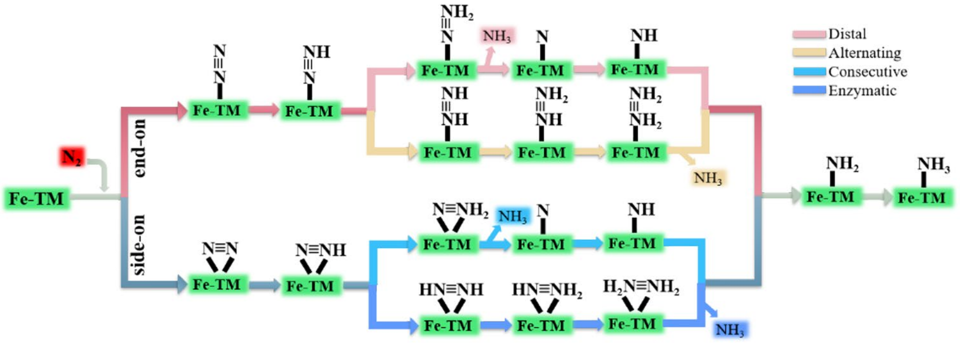

**Fig. 8** Schematic representation of the different mechanisms for NRR

attacks one N atom in $N_2$ molecule to produce a $NH_3$ molecule, then attacks the remaining N atom to produce another $NH_3$ molecule, and through the alternate and enzymatic mechanism, the proton-electron pair alternately attacks two nitrogen atoms and finally releases two $NH_3$ molecules in succession.

Figure 9 shows the Gibbs free energy change through different mechanisms at each step of the entire NRR process on the five kinds of selected catalysts. The PDS value of each pathway has been marked in each figure. Among them, for FeTi@Pc and FeZr@Pc, the fourth step of hydrogenation ($*NHNH_2+H^++e^- =*NH_2NH_2$) in the Alternating path after adsorbing $N_2$ molecules in the end-on configuration is difficult to complete, so for these two This kind of catalyst, only the Distal path will be considered in subsequent research. Under the functions of these two catalysts, the Gibbs free energy of NRR showed a downward trend, in which the PDS is the first hydrogenation reaction ($*N_2+H^++e^- =*N_2H$), and their values were 0.37 eV and 0.42 eV, respectively. For the other three catalysts (FeV@Pc, FeCu@Pc and FeTc@Pc), both Distal and Alternating paths are considered, but it is worth noting that for the Alternating path, the fourth hydrogenation step ($*NHNH_2+H^++e^- =*NH_2NH_2$) has a very high uphill Gibbs free energy change, which is also the decisive step in the entire Alternating path, with values of 1.23 eV, 0.98 eV and 1.22 eV, respectively. Compared with the Alternating path, their Distal path is more feasible, and the reaction process is generally downhill. As can be seen from Fig. 8c and e, on FeV@Pc and FeTc@Pc, $*N_2H$ forms $*NNH_2$ through protonation of the terminal path with a smaller upslope free energy value than *NHNH forms under the alternate path, indicating that in thermodynamics, the formation of $*NNH_2$ requires less energy than that of *NHNH. However, in Fig. 9d on FeCu@Pc, the biggest difference between the two paths lies in the fourth step of the hydrogenation reaction, where the Alternating path has a more corrected Gibbs free energy than the Distal path and is thus greatly hindered. Among them, under the action of FeV@Pc catalyst, the PDS of NRR is the second hydrogenation reaction with a value of 0.45 eV, and under the effects of FeCu@Pc and FeTc@Pc, the PDS of NRR is still the first hydrogenation reaction. The values are 0.38 eV and 0.59 eV, respectively. In summary, after the end-on configuration adsorbs $N_2$, NRR is thermodynamically more favorable through the Distal path. Only FeV@Pc can adsorb $N_2$ in side-on configuration, and in subsequent NRR, we consider two paths, continuous path and enzymatic path respectively. The variation paths of Gibbs free energy of two different mechanisms are shown in Fig. 9f. When $N_2$ is reduced to ammonia by the continuous mechanism on FeV@Pc catalyst, in addition to the hydrogenation reaction in the first step, which requires more energy, the fourth step is also required, but the enzymatic mechanism only increases the hydrogenation step in the first step, so for we chose the

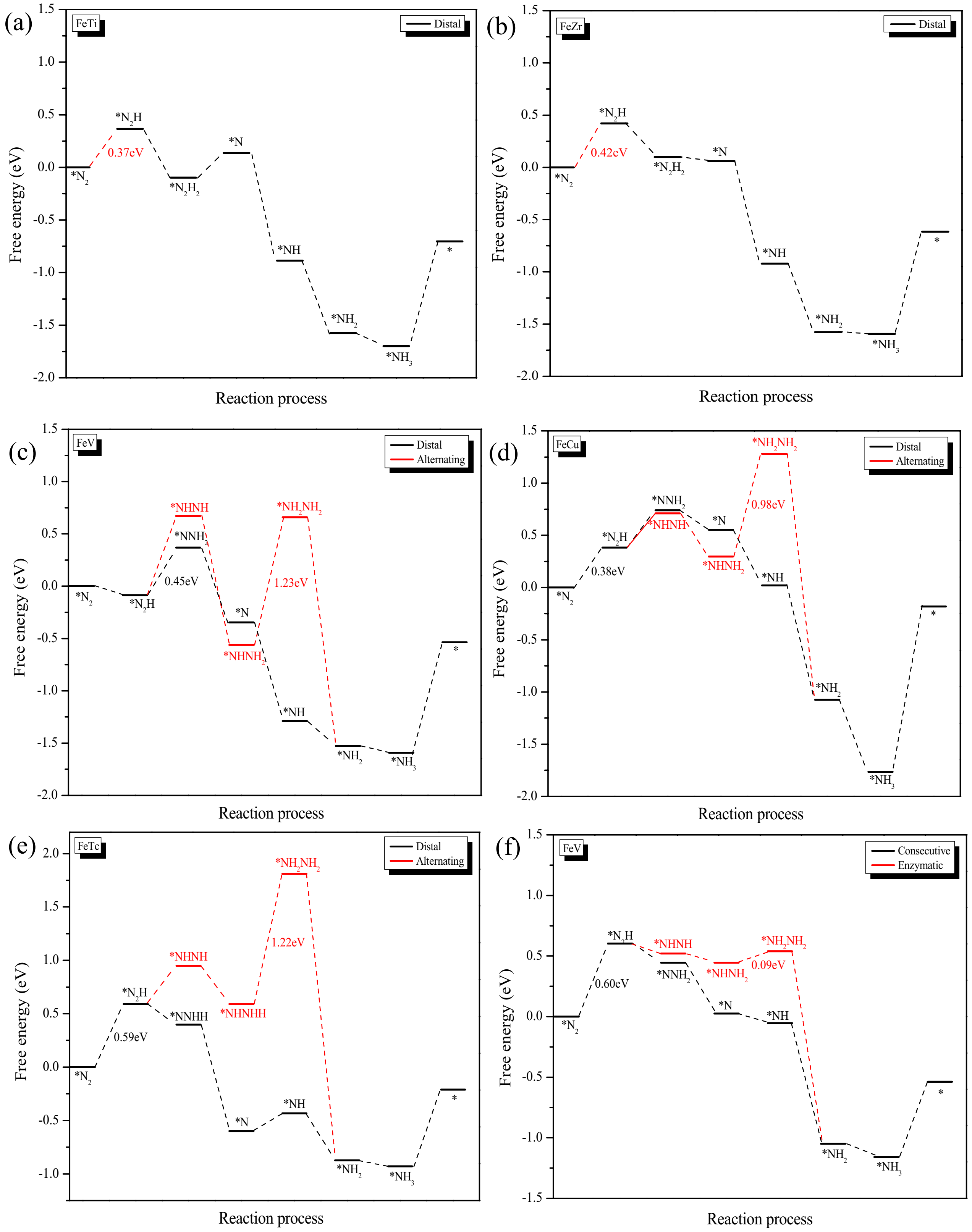

**Fig. 9** The Gibbs free energy change of NRR on **a** FeTi@Pc, **b** FeZr@Pc, **c** FeV@Pc, **d** FeCu@Pc, **e** FeTc@Pc and **f** FeV@Pc catalyst under different mechanisms. The free energy change value of PDSs have been marked

enzymatic mechanism. In this path, the entire free energy change process of NRR shows a downward slope, indicating that this route is possible for ammonia synthesis in terms of thermodynamics, where PDS is still the first step of hydrogenation, with 0.60 eV, but this value is still greater than the value of the PDS under the Distal mechanism. Finally, since the desorption of $NH_3$ plays an important role in the whole NRR process, it will affect the reuse of the catalyst, so we also plot the desorption energy of $NH_3$ in Fig. 9. As shown in the Fig. 9, the desorption of $NH_3$ is an endothermic reaction, and the energy required for the desorption of $NH_3$ over five catalyst systems (FeTi@Pc, FeV@Pc, FeCu@Pc, FeZr@Pc, and FeTc@Pc) are 0.99, 1.05, 1.58, 0.98, 0.72 eV, respectively. Among them, the $NH_3$ desorption energy of FeCu@Pc is slightly higher, and the $NH_3$ desorption energy of other catalyst systems is relatively moderate, which is similar or even lower than that in some theoretical studies [54, 77]. According to the above analysis, the Distal path is more feasible for the five kinds of selected catalysts. (The configurations of intermediate in the different mechanisms are shown in Fig. S2, and the energy of each intermediate is listed in Table S5).

To illustrate the intrinsic activity of the catalyst, we use the equation $U_L = -\Delta G_{PDS}/e$ about the limiting potential to calculate the $U_L$ value under the optimal path (Distal path) of the selected catalyst (the limit potential is the lowest negative potential that promotes PDS become exothermic). The corresponding $U_L$ values of FeTi@Pc, FeZr@Pc, FeV@Pc, FeCu@Pc, and FeTc@Pc are − 0.37, − 0.42, − 0.45, − 0.38, and − 0.59 V, respectively. Due to the presence of electrons, the applied electrode potential significantly affects the rate of proton-electron pair transfer in the protonation step. As shown in Fig. 10, after applying $U_L$ on the surface of the selected catalyst, all electron transfer steps can be downscaled, which is beneficial to the production of $NH_3$. Therefore, the Gibbs free energy curve will be significantly reduced when the potential is applied to the electrode. Through the above analysis, it can be concluded that among the five kinds of the selected catalysts, FeTi@Pc catalyzes NRR through the Distal path, displaying a least negative $U_L$ value of − 0.37 V, as shown in Fig. 10a.

### 3.5 Selectivity of FeTi@Pc Catalyst

In addition to high activity and high stability, an ideal catalyst also needs to have the ability to effectively inhibit the competitive reaction (HER), so as to obtain high Faraday efficiency of $NH_3$ synthesis. Therefore, we studied the catalytic selectivity of the selected catalyst. On most metal surfaces, the adsorption of hydrogen is easier than the adsorption of $N_2$, that is, the free energy of adsorbing hydrogen is less than the free energy of adsorbing $N_2$, which means that *H is likely to cover the metal surface to hinder the reaction activity. Moreover, the negative potential is easier to facilitate the H adsorption process involving one-step proton-electron transfer. If the electrode potential is increased, HER will play a dominant role in the reaction process until the adsorption of $N_2H$ [77]. In order to evaluate the selectivity of the catalyst, we calculated the activity of the hydrogen evolution reaction on the selected catalyst, as shown in Fig. 11a. At the same time, we also calculated the free energy for all the catalysts to adsorb *H and *$N_2H$ respectively, as shown in Fig. 11b. The darker the background color of the picture means the better the NRR catalytic activity, while the lighter the background color represents the better the catalyst activity for HER. Comparing the free energy value ($U_L$) of HER and NRR to determine the catalyst selectivity, $U_L$ (FeTi@Pc NRR) = − 0.37 V has a more favorable negative $U_L$ value than $U_L$ (FeTi@Pc HER) = − 0.53 V, indicating that FeTi@Pc can effectively inhibit HER and exhibit higher selectivity of NRR, which is consistent with the analysis results above, proving that FeTi@Pc is very promising for catalyzing NRR synthesis of $NH_3$. In addition to the adsorption on metal sites, we also studied all possible adsorption models of H on FeTi@Pc, and their structures are shown in Fig. S3, with corresponding adsorption energies ($\Delta G_{*H}$) marked in the figure. Where, except C8 site $\Delta G_{*H}$ value is negative, other H adsorption sites $\Delta G_{*H}$ value is positive, indicating that FeTi@Pc catalyst is more conducive to NRR. Even if C8 site $\Delta G_{*H}$ is less than 0, from another perspective, it indicates that H is more easily adsorb to C site without occupying the metal site and will not hinder the adsorption of $N_2$ by the metal site.To sum up, FeTi@Pc is an excellent catalyst with high selectivity in favor of NRR.

In order to verify the activity of our improved catalyst, we compared the $U_L$ value of the catalyst with Fe or other metal catalysts in Table 1. When comparing the catalyst with different metal catalysts, the results showed that FeTi@Pc had good catalytic activity, indicating that the way of doping transition metals we have studied can improve the performance of the catalyst. If this catalyst is compared with other iron-based catalysts (single-atom iron catalysts or homonuclear Fe catalysts), the results are still clear. It can be seen from the table that, $U_{L\ \text{max-FeTi@Pc}}$ (− 0.37 V) is significantly smaller than that of other monatomic iron catalysts, indicating that the catalytic activity of NRR monatomic iron catalyst can be further improved by rationally constructing the Fe-TM diatomic bimetallic catalyst.

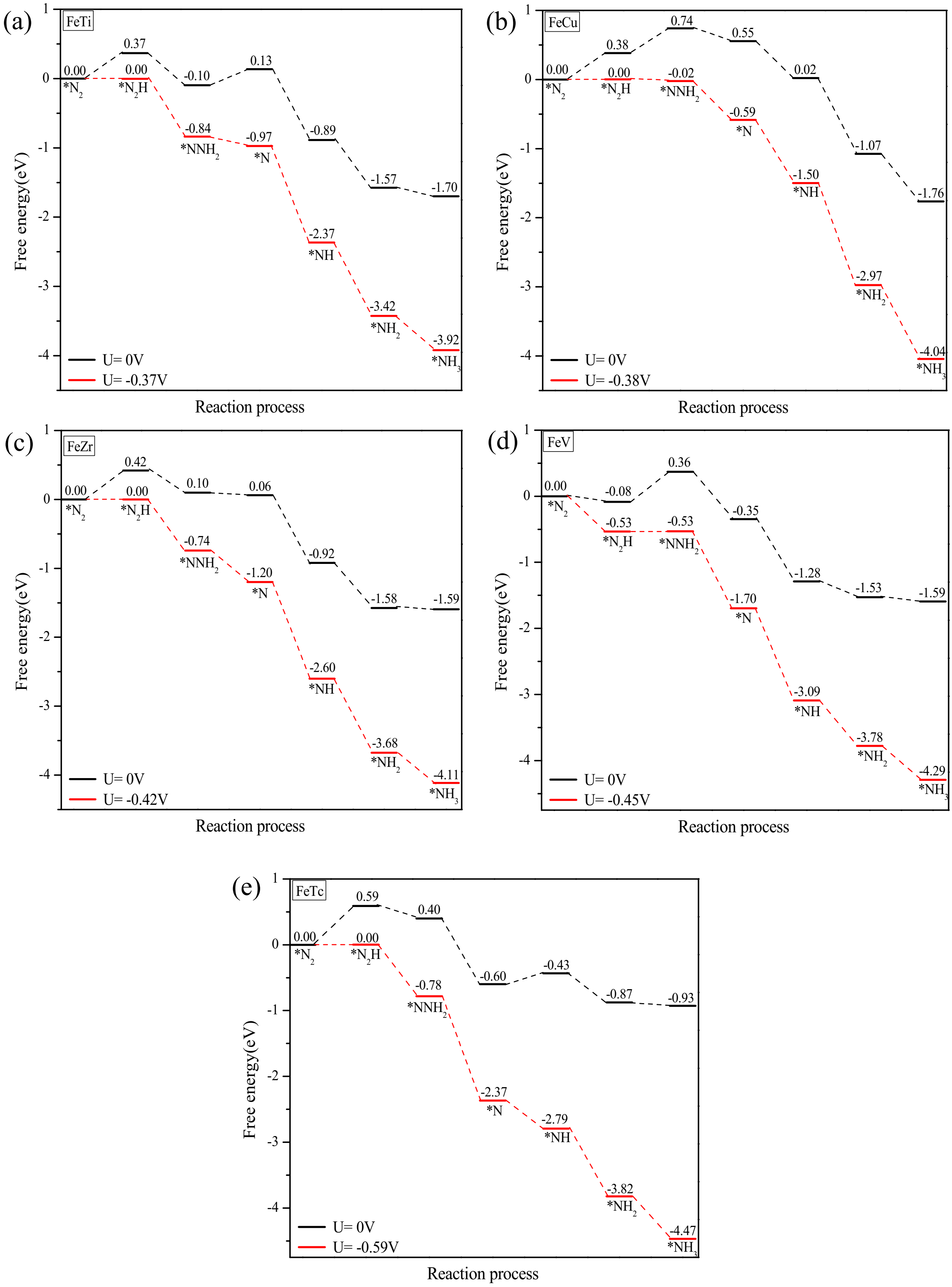

**Fig. 10** Free energy diagrams of NRR on **a** FeTi@Pc, **b** FeCu@Pc, **c** FeZr@Pc, **d** FeV@Pc and **e** FeTc@Pc along Distal mechanism. Black and red lines indicate free energy change for NRR at U = 0 V and U = – $\Delta G_{PDS}$/e, respectively

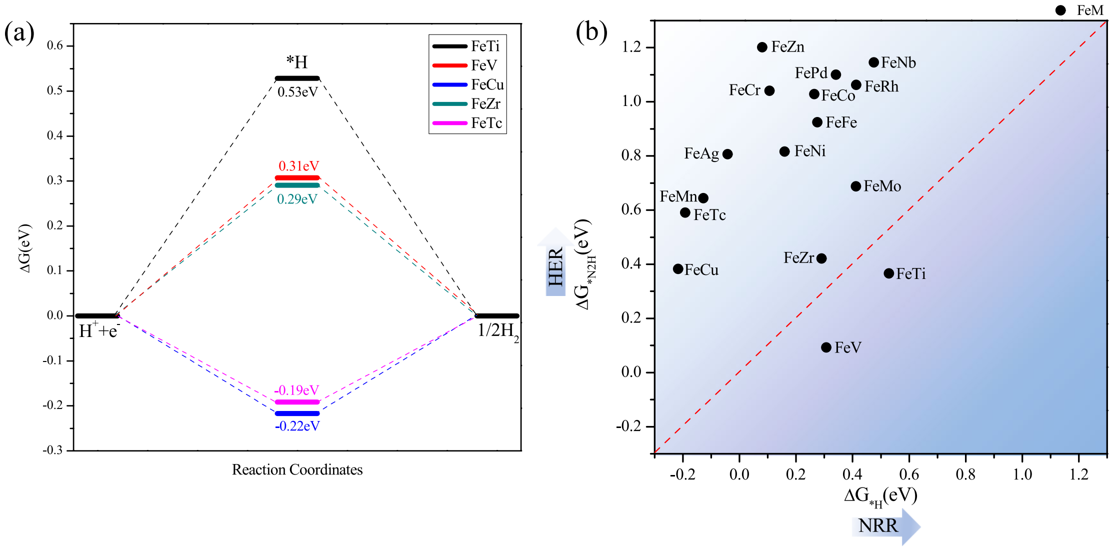

**Fig. 11** **a** Catalytic activity of hydrogen evolution reaction. **b** NRR activity and HER activity of FeTMs@Pc catalyst. (The red dotted line shows that $\Delta G_{*H}$ is equal to $\Delta G_{*N2H}$)

**Table 1** The Theoretical limiting potential of different catalysts for NRR

| Catalysts | Theoretical limiting potential $U_L$ (V) | Publication year |
|---|---|---|
| $Mo_2/C_2N$ | −0.51 | 2018[23] |
| $Ni_3$@GO | −1.23 | 2018[25] |
| Fe/GDY | −1.16 | 2019[21] |
| Fe (100) | −1.50 | 2019[66] |
| $Fe/N_4$-C | −1.69 | 2019[70] |
| Fe–Ti@GS | −0.88 | 2020[32] |
| $FeS_2$ | −0.45 | 2020[16] |
| Ru@GY | −0.43 | 2020[27] |
| $Fe\text{-}B_2N_2/G$ | −0.65 | 2021[71] |
| $Fe_2B_2$ | −0.44 | 2021[15] |
| V-PTC | −0.60 | 2021[26] |
| FeTi@Pc | −0.37 | This work |

## 4 Conclusion

In summary, the first and last step hydrogenation reaction, which may be the potential determination step, is used as the descriptor to screen out five catalysts among all the catalysts constructed. We used density functional theory to study the reaction paths, potential determining steps, Gibbs free energy changes, catalytic activity and selectivity of these five FeTMs@Pc electrocatalytic $N_2$ reduction reaction to ammonia. The results show that the catalytic activity is attributed to the optimized electronic structure and the strong interaction between the metal and the substrate. Compared with single-atomic iron catalysts, FeTMs@Pc has a lower Gibbs free energy change in the NRR potential determination step, and has more obvious advantages. The N≡N bond at the bimetallic catalytic active site was weakened by strong polarization, thus increasing the activity of NRR. Among the five FeTMs@Pc catalysts, FeTi@Pc showed the highest catalytic activity for NRR, with the Gibbs energy change of 0.37 eV. Electron-deficient Fe-Ti center plays a unique role in promoting $N_2$ fixation and activation for electron-rich species. The outermost electron arrangement of Ti element is $3d^24s^2$, and the number of electrons in its d shell is small, and such metal atoms have a strong binding force with nitrogen, which contributes to the subsequent $N_2$ reduction reaction. We expect that this work can encourage more experimental and theoretical efforts to study the synthesis of diatomic metal catalysts doped with phthalocyanine, and further explore their potential applications in various catalytic fields.

**Supplementary Information** The online version contains supplementary material available at https://doi.org/10.1007/s10562-022-04106-z.

**Acknowledgements** This work was financially supported by the Natural Science Foundation of Shanxi (Grant No.20210302123335), the Graduate Education Innovation Project of Shanxi Normal University (Grant No.2021XSY031).

## Declarations

**Conflict of interest** We declare that we have no financial and personal relationships with other people or organizations that can inappropriately influence our work.

## References

1. Rosca V, Duca M, Groot MT et al (2009) Nitrogen cycle electrocatalysis. Chem Rev 109:2209–2244
2. Wang L, Xia M, Wang H et al (2018) Greening ammonia toward the solar ammonia refinery. Joule 2:1055–1074
3. Guo J, Chen P (2017) Catalyst: $NH_3$ as an energy carrier. Chem 3:709–712
4. Kitano M, Inoue Y, Yamazaki Y et al (2012) Ammonia synthes is using a stable electride as an electron donor and reversible hydrogen store. Nat Chem 4:934–940
5. Legaré MA, Bélanger-Chabot G, Dewhurst RD et al (2018) Nitrogen fixation and reduction at boron. Science 359:896–899
6. Jackson RB, Canadell JG, Quéré CL et al (2016) Reaching peak emissions. Nat Clim Chang 6:7–10
7. Licht S, Cui B, Wang B et al (2014) Ammonia synthes is by $N_2$ and steam electrolysis in molten hydroxide suspensions of nanoscale $Fe_2O_3$. Science 345:637–640
8. VanderHam CJM, Koper MTM, Hetterscheid DGH (2014) Challenges in reduction of dinitrogen by proton and electron transfer. Chem Soc Rev 43:5183–5191
9. Shen H, Choi C, Masa J et al (2021) Electrochemical ammonia synthesis: mechanistic understanding and catalyst design. Chem 7:1–47
10. Zhang S, Zhao Y, Shi R et al (2019) Photocatalytic ammonia synthesis: recent progress and future. Energy Chem 1:100013
11. Shi L, Yin Y, Wang S et al (2020) Rational catalyst design for $N_2$ reduction under ambient conditions: strategies toward enhanced conversion efficiency. ACS Catal 10:6870–6899
12. Wang P, Chang F, Gao W et al (2017) Breaking scaling relations to achieve low-temperature ammonia synthesis through LiH-mediated nitrogen transfer and hydrogenation. Nat Chem 9:64–70
13. Cao N, Zheng G (2018) Aqueous electrocatalytic $N_2$ reduction under ambient conditions. Nano Res 11:2992–3008
14. Chen L, He C, Wang R et al (2021) Potential active sites of Mo single atoms for electrocatalytic reduction of $N_2$. Chin Chem Lett 32:53–56
15. Song W, Wang J, Fu L et al (2021) First-principles study on $Fe_2B_2$ as efficient catalyst for nitrogen reduction reaction. Chin Chem Lett 32:3137–3142
16. Du H, Yang C, Pu W et al (2020) Enhanced electrochemical reduction of $N_2$ to ammonia over pyrite $FeS_2$ with excellent selectivity. ACS Sustain Chem Eng 8:10572–10580
17. Pu C, Yu J, Fu L et al (2020) Two-dimensional $MgSiP_2$ with anisotropic electronic properties and good performances for Na-ion batteries. Chin Chem Lett 32:1081–1085
18. Xie J, Dong H, Cao X et al (2020) Computational insights into nitrogen reduction reaction catalyzed by transition metal doped graphene: comparative investigations. Mater Chem Phys 243:122622
19. Song Y, Li X, He C (2021) Porous carbon framework nested nickel foam as freestanding host for high energy lithium sulfur batteries. Chin Chem Lett 32:1106–1110
20. Zhou D, Li C, Yin F et al (2020) Two-dimensional 1T-$PS_2$ as a promising anode material for sodium-ion batteries with ultra-high capacity, low average voltage and appropriate mobility. Chin Chem Lett 31:2325–2329
21. Ma D, Zeng Z, Liu L et al (2019) Computational evaluation of electrocatalytic nitrogen reduction on TM single-, double-, and triple-atom catalysts (TM=Mn, Fe Co, Ni) based on graphdiyne monolayers. J Phys Chem C 123:19066–19076
22. Hu H, Yang H, Yang X et al (2020) Copper-sulfide cluster assembled architecture via in situ reaction. Chin Chem Lett 31:3213–3215
23. Li F, Chen L, Liu H et al (2019) Enhanced $N_2$-Fixation by engineering the edges of two-dimensional transition metal disulfides. J Phys Chem C 123:22221–22227
24. Yang Y, Liu J, Wei Z et al (2019) Transition metal-dinitrogen complex embedded graphene for nitrogen reduction reaction. ChemCatChem 11:2821–2827
25. Yang T, Tang S, Li X et al (2018) Graphene oxide-supported transition metal catalysts for di-nitrogen reduction. J Phys Chem C 122:25441–25446
26. Li B, Du W, Wu Q et al (2021) Coronene-based 2D metal-organic frameworks: a new family of promising single-atom catalysts for nitrogen reduction reaction. J Phys Chem C 125:20870–20876
27. Arachchige LJ, Xu Y, Dai Z et al (2020) Theoretical investigation of single and double transition metals anchored on graphyne monolayer for nitrogen reduction reaction. J Phys Chem C 124:15295–15301
28. Ma D, Wang Y, Liu L et al (2021) Electrocatalytic nitrogen reduction on the transition-metal dimer anchored N-doped graphene: performance prediction and synergetic effect. Phys Chem Chem Phys 23:4018–4029
29. Wei Z, He J, Yang Y et al (2021) Fe, V-co-doped $C_2N$ for electrocatalytic $N_2$-to-$NH_3$ conversion. J Energy Chem 53:303–308
30. Qian Y, Liu Y, Zhao Y et al (2020) Single vs double atom catalyst for $N_2$ activation in nitrogen reduction reaction: a DFT perspective. EcoMat 2:12014
31. Zhang H, Cui C, Luo Z (2020) $MoS_2$-Supported $Fe_2$ clusters catalyzing nitrogen reduction reaction to produce ammonia. J Phys Chem C 124:6260–6266
32. Yang W, Huang H, Ding X et al (2020) Theoretical study on double-atom catalysts supported with graphene for electroreduction of nitrogen into ammonia. Electrochim Acta 335:135667
33. Liang Z, Liu C, Chen M et al (2020) Theoretical screening of di-metal atom (M=Fe Co, Ni, Cu, Zn) electrocatalysts for ammonia synthesis. Int J Hydrogen Energ 45:31881–31891
34. Guo X, Du H, Qu F et al (2019) Recent progress in electrocatalytic nitrogen reduction. J Mater Chem A 7:3531–3543
35. Chen Z, Chen L, Yang C et al (2019) Atomic (single, double, and triple atoms) catalysis: frontiers, opportunities, and challenges. J Mater Chem A 7:3492–3515
36. Minteer SD, Christopher P, Linic S (2019) Recent developments in nitrogen reduction catalysts: a virtual issue. ACS Energy Lett 4:63–166
37. Chen Z, Yan J, Jiang Q (2019) Single or double: which is the altar of atomic catalysts for nitrogen reduction reaction. Small Method 3:1800291
38. Xu Z, An C, Zhang Z et al (2018) Double-atom catalysts: transition metal dimer-anchored $C_2N$ monolayers as $N_2$ fixation electrocatalysts. J Mater Chem A 6:18599–18604
39. Liu J, Ma X, Li Y et al (2018) Heterogeneous $Fe_3$ single-cluster catalyst for ammonia synthes is via an associative mechanism. Nat Commun 9:1610
40. Han X, Lang Z, Yan L et al (2019) Atomic Nb anchoring on graphdiyne as a new potential electrocatalyst for nitrogen fixation: a computational view. Adv Theory Simul 2:1900132
41. Geng Z, Liu Y, Kong X et al (2018) N2 electrochemical reduction: achieving a record-high yield rate of 120.9 μgNH3 mgcat.−1 h−1 for N2 electrochemical reduction over Ru single-atom catalysts. Adv Mater 30:1803498
42. Tao H, Choi C, Ding L et al (2019) Nitrogen fixation by Ru single-atom electrocatalytic reduction. Chem 5:204–214
43. Guo X, Chen S, Wang H et al (2019) Single-atom molybdenum immobilized on photoactive carbon nitride as efficient photocatalysts for ambient nitrogen fixation in pure water. J Mater Chem A 7:19831–19837

44. Zang W, Yang T, Zou H et al (2019) Copper single atoms anchored in porous nitrogen-doped carbon as efficient pH-universal catalysts for the nitrogen reduction reaction. ACS Catal 9:10166–11017
45. Varela AS, Ju W, Bagger A et al (2019) Electrochemical reduction of $CO_2$ ($CO_2RR$) on metal-nitrogen-dopedcarbon (M-N-C) catalysts. ACS Catal 9:7270–7284
46. Ren W, Tan X, Yang W et al (2019) Isolated diatomic Ni-Fe metal-nitrogen sites for synergistic electroreduction of $CO_2$. Angew Chem Int Ed 58:6972–6976
47. Li Z, He H, Cao H et al (2019) Atomic Co/Ni dual sites and Co/Ni alloy nanoparticles in N-doped porous Janus-like carbon frameworks for bifunctional oxygen electrocatalysis. Appl Catal B 240:112–121
48. Luo Q, Zhang W, Fu C et al (2018) Single Pd atom and Pd dimer embedded graphene catalyzed formic acid dehydrogenation: a first-principles study. Int J Hydrogen Energy 43:6997–7006
49. Jiang J, Sun F, Zhou S et al (2018) Atomic-level insight into super-efficient electrocatalytic oxygen evolution on iron and vanadium co-doped nickel (oxy) hydroxide. Nat Commun 9:1–12
50. Yu L, Li F, Zhao J et al (2022) Revisiting catalytic performance of supported metal dimers for oxygen reduction reaction via magnetic coupling from first principles. Adv Powder Technol 1:100031
51. Cao L, Shao Y, Pan H et al (2020) Designing efficient dual-metal single-atom electrocatalyst TMZnN6 (TM = Mn, Fe Co, Ni, Cu, Zn) for oxygen reduction reaction. J Phy Chem C 124:11301–11307
52. Li Y, Su H, Chan S et al (2015) $CO_2$ electroreduction performance of transition metal dimers supported on graphene: a theoretical study. ACS Catal 5:6658–6664
53. He T, Puente-Santiagoc AR, Du A (2020) Atomically embedded asymmetrical dual-metal dimers on N-doped graphene for ultra-efficient nitrogen reduction reaction. J Catal 388:77–83
54. Li H, Zhao Z, Cai Q et al (2020) Nitrogen electroreduction performance of transition metal dimers embedded into N-doped graphene: a theoretical prediction. J Mater Chem A 8:4533–4543
55. Liu Y, Song B, Huang C, Yang L (2022) Dual transition metal atoms embedded N-doped graphene for electrochemical nitrogen fixation under ambient conditions. J Mater Chem A 15:4039–4047
56. d'Alessandro N, Liberatore L, Tonucci L et al (2001) Direct synthesis of adipic acid by mono-persulfate oxidation of cyclohexane, cyclohexanone or cyclohexanol catalyzed by water-soluble transition-metal complexes. New J Chem 25:1319–1324
57. Grootboom N, Nyokong T (2002) Iron perchloro phthalocyanine and tetrasulfo phthalocyanine catalyzed oxidation of cyclohexane using hydrogen peroxide chloroperoxybenzoic acid and tert-butylhydroperoxide as oxidants. J Mol Catal A Chem 179:113–123
58. Karandikar P, Chandwadkar AJ, Agashe M et al (2006) Liquid phase oxidation of alkanes using Cu/Co-perchloro phthalocyanine immobilized MCM-41 under mild reaction conditions. Appl Catal A-Gene 297:220–230
59. Brown ES, Robinson JR, Mccoy AM et al (2011) Efficient catalytic cycloalkane oxidation employing a "helmet" phthalocyaninato iron (III) complex. Dalton Trans 40:5921–5925
60. Bıyıklıoğlu Z, Saka ET, Gökçe S et al (2013) characterization and investigation of homogeneous oxidation activities of peripherally tetra-substituted Co (II) and Fe (II) phthalocyanines: oxidation of cyclohexene. J Mol Catal A-Chemical 378:156–163
61. Morlanés N, Takanabe K et al (2016) Simultaneous reduction of $CO_2$ and splitting of $H_2O$ by a single immobilized cobalt phthalocyanine electrocatalyst. ACS Catal 6:3092–3095
62. Kumar P, Santhakumar K, Shin PK et al (2013) Improving the photovoltaic parameters of organic solar cell using soluble copper phthalocyanine nanoparticles as a buffer layer. Jpn J Appl Phys 53:01AB06
63. Li R, Huang L, Lin Z (2014) Study on the synthesis and in vitro photodynamic anti-cancer activity of tetra(trifluoroethoxy) germanium phthalocyanine. Chinese J Struc Chem 33:1081–1090
64. Zhang X, Wu Z, Zhang X (2017) Highly selective and active $CO_2$ reduction electrocatalysts based on cobalt phthalocyanine/carbon nanotube hybrid structures. Nat Commun 8:1–8
65. Han N, Wang Y, Ma L (2017) Supported cobalt polyphthalocyanine for high-performance electrocataltyic $CO_2$ reduction. Chem 3:652–664
66. Sharad M, Gholamreza R, Michael JJ (2019) Elementary kinetics of nitrogen electroreduction on Fe surfaces. J Chem Phys 150:041708
67. Skúlason E, Bligaard T, Gudmundsdottir S et al (2012) A theoretical evaluation of possible transition metal electro-catalysts for $N_2$ reduction. Phys Chem Chem Phys 14:1235–1245
68. Liu Q, Wang Y, Hu Z et al (2021) Iron-based single-atom electrocatalysts: synthetic strategies and applications. RSC Adv 11:3079–3095
69. He C, Wu Z, Zhao L et al (2019) Identification of $FeN_4$ as an efficient active site for electrochemical $N_2$ reduction. ACS Catal 9:7311–7317
70. Lü F, Zhao S, Guo R et al (2019) Nitrogen-coordinated single Fe sites for efficient electrocatalytic $N_2$ fixation in neutral media. Nano Energy 61:420–427
71. Jiao D, Liu YJ, Cai Q et al (2021) Coordination tunes activity and selectivity of nitrogen reduction reaction on single-atom iron catalysts: a computational study. J Mater Chem A 9:1240–1251
72. Guo X, Gu J, Hu X et al (2019) Coordination tailoring towards efficient single-Atom catalysts for $N_2$ fixation: a case study of iron-nitrogen-carbon (Fe@N-C) systems. Catal Today 350:91–99
73. Perdew JP, Burke K, Ernzerhof M (1996) Generalized gradient approximation made simple. Phys Rev Lett 77:3865–3868
74. Hay PJ, Wadt WR (1985) Generalized gradient approximation made simple. J Chem Phys 82:299–310
75. Nørskov JK, Rossmeisl J, Logadottir A et al (2004) Origin of the overpotential for oxygen reduction at a fuel-cell cathode. J Phys Chem B 108:17886–17892
76. Zhu YA, Chen D, Zhou XG et al (2009) DFT studies of dry reforming of methane on Ni catalyst. Catal Today 148:260–267
77. Guo X, Gu J, Lin S et al (2020) Tackling the activity and selectivity challenges of electrocatalysts toward the nitrogen reduction reaction via atomically dispersed biatom catalysts. J Am Chem Soc 142:5709–5721
78. Montoya JH, Tsai C, Vojvodic A et al (2015) The challenge of electrochemical ammonia synthesis: a new perspective on the role of nitrogen scaling relations. Chem Sus Chem 8:2180–2186
79. Guo C, Ran J, Vasileff A et al (2018) Rational design of electrocatalysts and photo (electro) catalysts for nitrogen reduction to ammonia ($NH_3$) under ambient conditions. Energy Environ Sci 11:45
80. Ling C, Ouyang Y, Li Q et al (2019) A general two-step strategy-based high-throughput screening of single atom catalysts for nitrogen fixation. Small Methods 3:1800376
81. Li L, Wang X, Guo H et al (2019) Theoretical screening of single transition metal atoms embedded in MXene defects as superior electrocatalyst of nitrogen reduction reaction. Small Methods 3:1900337
82. Jia C, Wang Q, Yang J et al (2022) Toward rational design of dual-metal-site catalysts: catalytic descriptor exploration. ACS Catal 12:3420–3429
83. Yang M, Wang Z, Jiao D et al (2022) Tuning precise numbers of supported nickel clusters on graphdiyne for efficient $CO_2$ electroreduction toward various multi-carbon products. J Energy Chem 69:456–465

84. Wang S, Shi L, Bai X et al (2020) Highly efficient photo-/electrocatalytic reduction of nitrogen into ammonia by dual-Metal sites. ACS Cent Sci 6:1762–1771
85. Sun S, Zhou X, Cong B et al (2020) Tailoring the d-band centers endows $(Ni_xFe_{1-x})_2P$ nanosheets with efficient oxygen evolution catalysis. ACS Catal 10:9086–9097
86. Deng T, Cen C, Shen H et al (2020) Atom-pair catalysts supported by N-doped graphene for the nitrogen reduction reaction: d-band center-based descriptor. J Phys Chem Lett 11:6320–6329
87. He F, Wang Z, Wei S et al (2020) Adsorption and catalytic activation of $N_2$ molecule on iron dimer supported by different two-dimensional carbon-based substrates: a computational study. Appl Surf Sci 506:144943
88. Arachchige LJ, Xu Y, Dai Z et al (2021) Double transition metal atoms anchored on graphdiyne as promising catalyst for electrochemical nitrogen reduction reaction. J Mater Sci Technol 77:244–251

**Publisher's Note** Springer Nature remains neutral with regard to jurisdictional claims in published maps and institutional affiliations.

Springer Nature or its licensor holds exclusive rights to this article under a publishing agreement with the author(s) or other rightsholder(s); author self-archiving of the accepted manuscript version of this article is solely governed by the terms of such publishing agreement and applicable law.